# A Comprehensive Comparison of Voltage and Current Control Techniques for Three-Phase VSI Converters

Daniel F. S. Fernandes[*,1], Rui F. O. Costa[1], Luis A. M. Barros[1,2], Delfim Pedrosa[1,2], João L. Afonso[1,2], J. G. Pinto[1,2]

[1] Department of Industrial Electronics – University of Minho, Guimarães – Portugal
[2] Centro ALGORITMI – University of Minho, Guimarães – Portugal

*Correspondence: a81700@alunos.uminho.pt

**Abstract.** Converting electrical energy from direct current to alternate current, or vice versa, is one of the most frequently performed tasks in today's electrical systems. The Voltage Source Inverter (VSI) is the most widely used topology to accomplish this task. This paper compares the performance of three control algorithms for voltage source inverter (VSI) with PI, PR and MP control algorithms were applied for voltage control and current control. For voltage control the VSI synthesizes the sinusoidal voltage system for an islanded application. In current control the VSI injects energy into the power grid by synthesizing sinusoidal currents. A general comparison is made of the performance of the three control algorithms under the presented conditions, helping to choose the control algorithm to use in a given application.

**Keywords:** Voltage Source Inverter, Current Control, Voltage Control.

## 1    Introduction

Nowadays, electrical energy is indispensable for the execution of many tasks. With their increasing relevance, power electronics converters have become the focus of research to improve their performance and applicability. Power electronics converters can be grouped into four categories: DC-DC, DC-AC, AC-DC and AC-AC [1]. Within each category there are several topologies aimed at the most varied applications related to the production, transport and distribution of electrical energy (transformers, power generation systems, power grid interfaces for alternative energy resources such as solar photovoltaic panels, wind turbines and energy storage systems) [2]-[3], industry (motor drive systems) [4], household activities (air conditioners, computers, electric vehicle chargers) [5] among others.

Regarding the DC-AC power converters, these can be classified according to their power supply, being divided into two large groups: voltage source inverter (VSI) and current source inverter (CSI) [6].

The VSI are the most used. Through the control algorithm it is possible to adjust the output amplitude and frequency. The VSI are used in various applications such as

AC motor adjustable speed drives or interfacing energy production systems from renewable sources with the power grid [7].

Although it is widely used, there is a gap in the literature in explaining and comparing control algorithms for VSI. The schematic in Fig. 1 (a) shows the voltage-controlled VSI used in this study where the converter generates the sinusoidal voltage system responsible for feeding a set of loads islanded from the power grid. The Fig. 1 (b) shows the block diagram of the current-controlled VSI assembly used in this work, where it is responsible for injecting energy into the power grid.
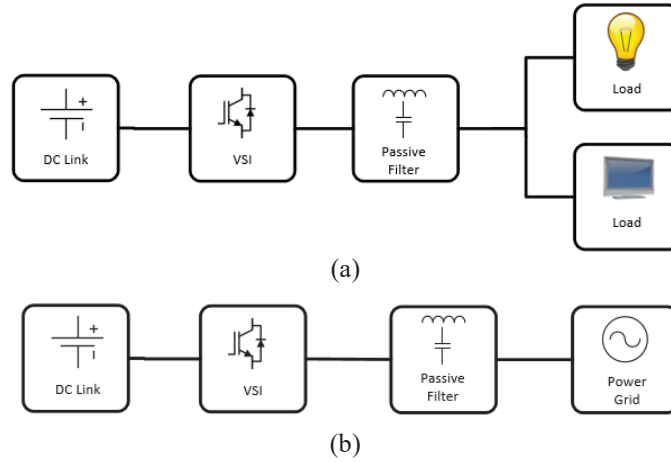


(a)



(b)

**Fig. 1.** Block diagram of the VSI applications using: (a) voltage-control; (b) current-control.

In this paper, three control algorithms for VSI are described and implemented: Proportional Integral (PI), Proportional Resonant (PR) and Model Predictive (MP). The objective of the paper is to compare the performance of these three algorithms in current-control and voltage-control modes.

This document is organized into five sections, as follows: Section 1 provides an introduction to the subject; Section 2 describes the VSI topology and its applications; in Section 3 the three control algorithms used, the PI, PR and MP, are described; in Section 4 the simulation results for the VSI controlled by voltage and current are presented; and, finally, in Section 5, the main conclusions and some ideas for future work are presented.

## 2 VSI Converter Topologies

The diagram of a VSI with three legs and four wires is represented in Fig. 2. This VSI requires a DC-Link division to generate a midpoint. The main advantage of this topology is the fact that this converter can control the voltage of each phase in relation to the neutral point. With its connection to the system neutral, a return path for the neutral current is created, which is an asset in unbalanced systems or for compensating power quality (PQ) problems. For its correct operation, it is necessary to ensure that the voltages $V_{DC1}$ and $V_{DC2}$ have similar values.
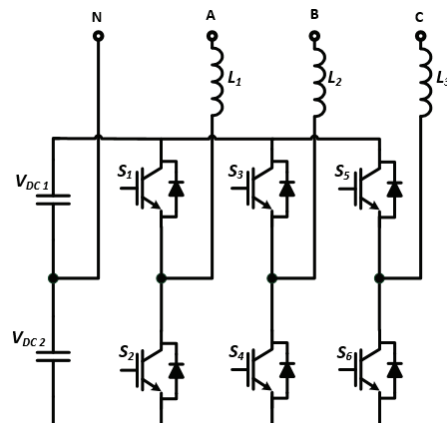
**Fig. 2.** VSI with 3 legs and 4 wires with a split capacitor in the DC-Link.

Since this type of converter is bidirectional (it can transfer energy from the DC side to the AC side or from the AC side to the DC side), its use is quite wide. In [8] is a study of the application of a 3-leg 4-wire VSI with split capacitor in the charging of an electric vehicle was presented.

In [9] the author used a 3 leg and 3 wire VSI as a shunt active filter in order to compensate the current harmonics in a three-phase power grid system. The author was able to significantly reduce the Total Harmonic Distortion (THD%) of the currents on the power grid side.

This converter is widely used in renewable energy applications. In [10] is used to inject the energy produced by an array of PV modules into the power grid. In [11] the author used a VSI topology for a wind power system based on a six-phase permanent magnet synchronous generator with fixed switching frequency.

Another application of the VSI is in motor control. In [12] a VSI based on Silicon Carbide Metal Oxide Semiconductor Field Effect Transistor (SiC MOSFET) was developed in order to feed a squirrel cage induction motor controlled using a constant *V/f* (it is an induction motor control method which ensures the output voltage proportional with the frequency) control achieving good results under different motor operating conditions.

## 3 Voltage and Current Control Techniques

In this topic the different control algorithms implemented for the comparative study are presented and analyzed. For each one of them, a block diagram of its constitution or the mathematical equation for its implementation is presented.

### 3.1 Proportional Integral (PI) Control

The PI voltage control technique is based on the calculation of the error, $v_{error}$, between the reference voltage, $v_{ref}$, and the converter output voltage, $v_{out}$. The error resulting

from this operation is multiplied by a proportional gain, $K_P$, and an integral gain, $K_I$. The resulting variable, $v_{control}$, is used to synthesize the command signals of the semi-conductors to be controlled. In Fig. 3 the block diagram of the PI voltage control algorithm is represented. For the current control, the diagram is similar, replacing the voltage signals with their respective current signals.
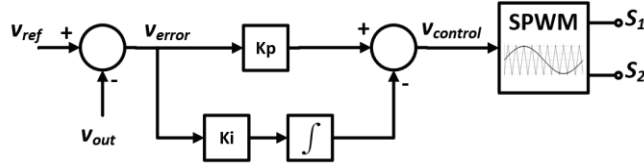


**Fig. 3.** Block diagram of the PI voltage-control algorithm.

In [13] a modified PI control was applied to a brushless DC motor (BLDC) with the objective of contributing to the application of this type of motor in electric vehicles.

## 3.2 Proportional Resonant (PR) Control

In Fig. 4 the diagram of the PR controller is represented. This control algorithm uses the error, $v_{error}$, between the reference signal, $v_{ref}$, and the synthesized signal, $v_{out}$, as inputs. The resulting value $v_{error}$ is multiplied by a resonant gain, $K_S$, that will be the input from a second order generalized integrator (SOGI) [14]. Its output is added to the error multiplied by a proportional gain, $K_P$, resulting in the signal that will be the input to the sinusoidal pulse width modulation (SPWM) technique, $v_{control}$. The $\omega_0$ constant represents the fundamental frequency of the signal to be synthesized. For 50 Hz applications, this value is approximately 314 rad/s ($2 \pi f$). For the current control, the diagram is similar, replacing the voltage signals with their respective current signals.
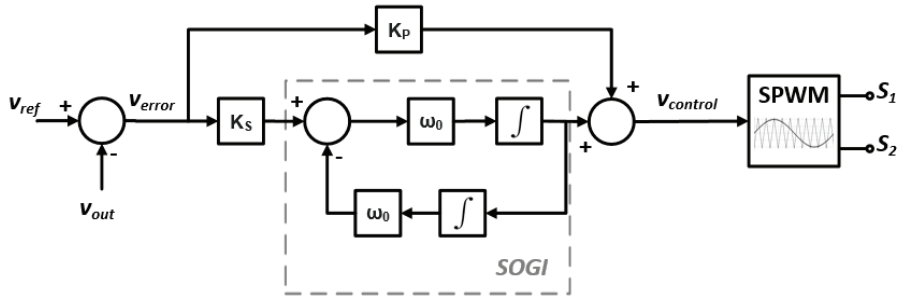


**Fig. 4.** Block diagram of the PR control algorithm.

In the literature there are some applications of this algorithm. For example, in [15] this algorithm was applied to a shunt active power filter used in unbalanced systems. The results prove its good operation for compensation of harmonics and neutral currents. In [16] PR control was applied to an inverter in order to inject the energy produced by a photovoltaic module into the power grid.

### 3.3    Model Predictive (MP) Control

The MP control technique is based on the electrical model of the system to predict the future behavior of the variables to be controlled, taking advantage of the finite number of possible switching states for a static energy converter (such as the VSI) [17]. In the literature there are several predictive controls [18]-[19]-[20].

This control algorithm has the advantage of having no gains in its closed loop, depending only on the constituent elements of the system and the quality of the electrical model used. This allows the control system to have a good response to the unpredictability of the loads that can be connected to the system [17].

In this work the control algorithm described below was used. The explanation is oriented towards a single-phase VSI since, for the case of a three-phase converter, it is only necessary to replicate the control for the remaining phases of the system. In Fig. 5 is the electrical representation of a grid connected single-phase VSI.
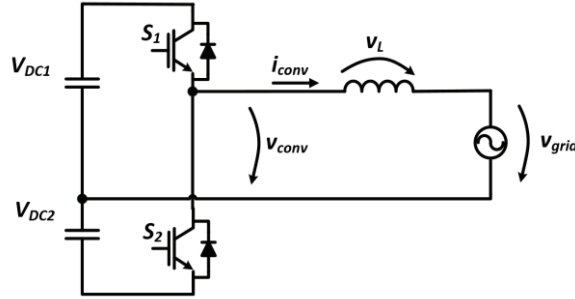


**Fig. 5.** Electrical diagram of a single-phase inverter connected to the power grid.

Considering the model presented in Fig. 5 and applying Kirchhoff's voltage laws, it is possible to deduce the equation (1). The converter output voltage ($v_{conv}$) results from the sum of the voltage at the inductor terminals ($v_L$) and the power grid voltage ($v_{grid}$). This model assumes that the inductor internal resistance is very small and can be neglected.

$$v_{conv} = v_{grid} + v_L \tag{1}$$

Using an equation characteristic of the voltage in an inductor, $v_L$, it is possible to obtain the equation (2).

$$v_{conv} = v_{grid} + L\frac{di_{conv}(t)}{dt} \tag{2}$$

This control is applied in closed-loop. The error current ($i_{error}$) is calculated from the subtraction of the converter output current ($i_{conv}$) and the reference current ($i_{ref}$), as represented in (3).

$$i_{error} = i_{ref} - i_{conv} \tag{3}$$

By updating the equation (2) of the electrical model of the system with the equation (3) of the reference current, it is possible to obtain the equation (4)

$$v_{conv} = v_{grid} - L\frac{di_{error}(t)}{dt} + L\frac{di_{ref}(t)}{dt} \tag{4}$$

To cancel the current error ($i_{error}$), the controller must allow the converter to generate a voltage that, when applied to the inductor, causes a current with equal amplitude but in phase opposition to the calculated in the equation (3). So, it is possible to obtain the equation (5).

$$v_{Conv} = v_{grid} + L\frac{di_{error}(t)}{dt} + L\frac{di_{ref}(t)}{dt} \tag{5}$$

Microcontrollers cannot work in the continuous domain. They have a minimum time between samples which makes them discrete domain devices. Converting equation (5) to the discrete domain, it was obtained equation (6), where $T_a$ is the acquisition period.

$$v_{conv}[k] = v_{grid}[k] + \frac{L}{T_a}(2\,i_{ref}[k] - i_{ref}[k-1] - i_{conv}[k]) \tag{6}$$

The same principle and equations can be applicate to the voltage-controlled MP by replacing the reference and produced currents by the reference and produced voltages.

## 4 Simulation Results

This chapter presents the simulations carried out in this work. These are divided into two subchapters: voltage-controlled VSI and current-controlled VSI. In the simulations performed for this paper, equal parameters were used to make a fair comparison between algorithms. Table 1 shows the general parameters used in these simulations.

Table 1. General parameters of the simulations.

| Parameter | Value | Unit |
|---|---|---|
| Inductors $L_1$, $L_2$, $L_3$ | 5 | mH |
| Switching Frequency | 20 | kHz |
| Sampling Frequency | 40 | kHz |
| Upper Peak of the Triangular Carrier | 3750 | - |
| Lower Peak of the Triangular Carrier | 0 | - |

### 4.1 Voltage Controlled VSI

In the presented simulation, the VSI is controlled by voltage. A group of loads has been added, as shown in Fig. 6. A configuration in star of 3 resistive loads of 50 Ω each was used. Regarding the nonlinear load, it was used a three-phase full-bridge diode rectifier with a RC load. The capacitor used was 500 µF and the resistor has the value of 200 Ω. An LC filter was placed at the output of the converter, where the inductor is 5 mH, the capacitor is 30 µF and the resistor is 2.2 Ω.
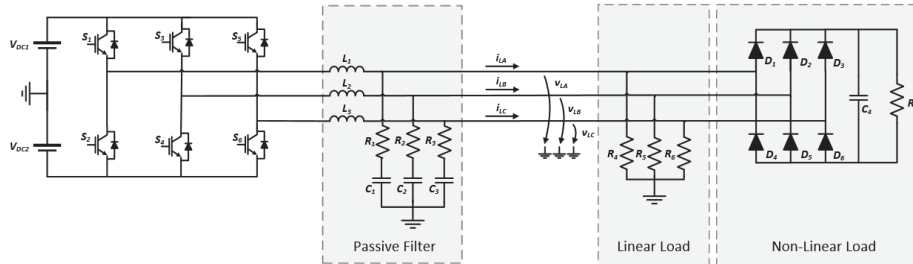
**Fig. 6.** Electrical diagram of the circuit used for the voltage-controlled VSI study.

During this study are used different voltage control algorithms applied to the VSI. The objective is to see the different behaviors of the different controls with linear loads and nonlinear loads connected to the system. The control algorithms used in this simulation are the PI, PR and MP. The simulation conditions are the same for the three voltage control algorithm under study. In this simulation, the linear load is connected at 0.2 s and at 0.25 s the nonlinear load is added until the end of the simulation time. For the nonlinear load is used a pre-charge circuit to charge the capacitor in such a way as not to cause disturbances in the system at its connection.

**PI Voltage Control Algorithm**

The first control algorithm implemented was PI. The simulation starts with the linear load connected to the electrical system and after 0.25 s a nonlinear load is added. From that time the system is powering the linear load and the nonlinear load. With this simulation, it is intended to verify the differences in the behavior of the voltage control algorithm with the two different loads and seeing the behavior of the control when the load addiction occurs. In Fig. 7 are presented the results of this simulation with the linear and nonlinear loads. These results are obtained using a $K_p$ of 130 and a $K_i$ of 5.
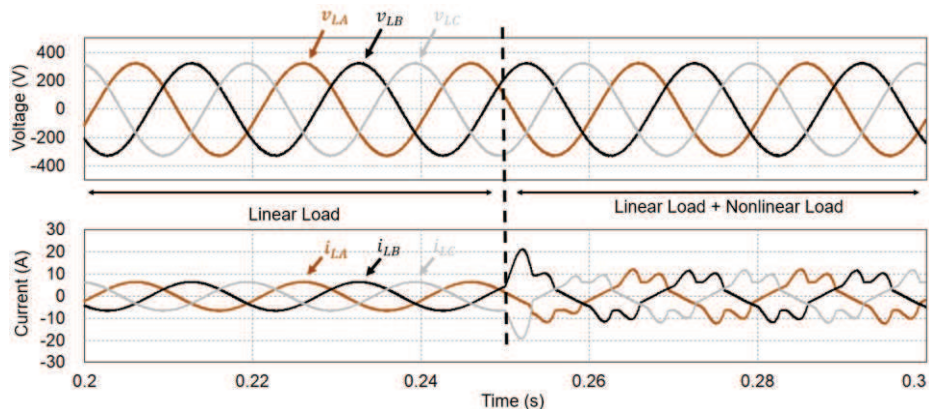


**Fig. 7.** VSI output voltages and load currents with PI voltage control algorithm.

Analyzing the obtained results, it is possible to conclude that the PI control algorithm works correctly not only with a linear load but also with a nonlinear load. The voltage THD increased a little bit with a nonlinear load comparing with the results obtained with the linear load. In Table 2 is presented the THD% voltage results during this simulation.

**Table 2.** PI voltage control algorithm THD% comparison using different loads.

| Load | Voltage | THD% |
|---|---|---|
| | $v_{LA}$ | 1.18% |
| Linear | $v_{LB}$ | 1.14% |
| | $v_{LC}$ | 1.14% |
| | $v_{LA}$ | 1.27% |
| Linear + Nonlinear | $v_{LB}$ | 1.23% |
| | $v_{LC}$ | 1.23% |

**PR Voltage Control Algorithm**

The second control algorithm implemented was PR. The simulation starts with the linear load connected to the system and after 0.25 s the load addiction occurs, becoming the linear load and the nonlinear load connected to the system. In Fig.8 are presented the results of this simulation with the linear and nonlinear loads. These results are obtained using a $K_p$ of 200 and a $K_s$ of 1000.
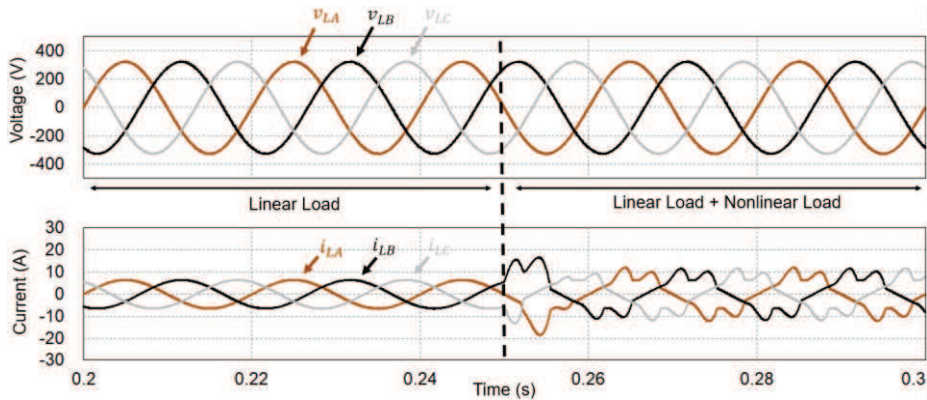


**Fig. 8.** VSI output voltages and load currents with PR voltage control algorithm.

Analyzing the obtained results, it is possible to conclude that the PR voltage control algorithm works correctly with a linear load as well as with a nonlinear load on the system. The THD% voltage results are presented in Table 3.
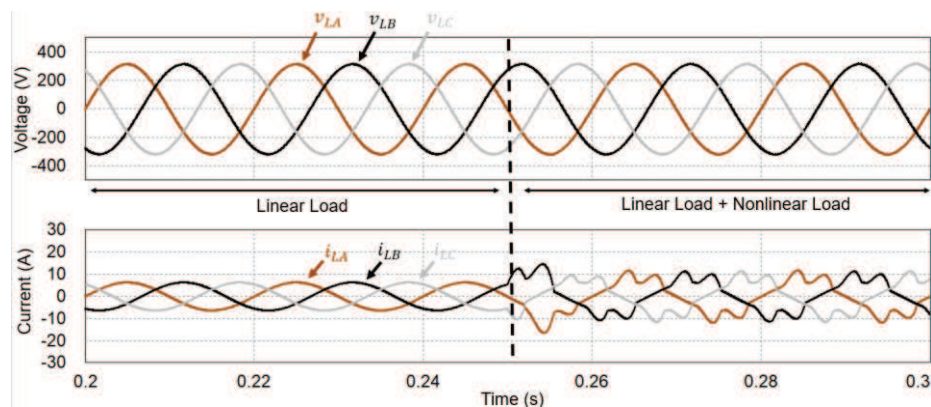
**Table 3.** PR voltage control THD% comparison using different loads.

| Load | Voltage | THD% |
|---|---|---|
| | $v_{LA}$ | 1.16% |
| Linear | $v_{LB}$ | 1.06% |
| | $v_{LC}$ | 1.09% |
| | $v_{LA}$ | 1.25% |
| Linear + Nonlinear | $v_{LB}$ | 1.16% |
| | $v_{LC}$ | 1.18% |

The THD% voltage increased when the nonlinear load is connected to the system comparing with the results with a linear load. Although, the THD% results are very satisfactory for both loads. Comparing this control to the results obtained for the PI control, they are very similar, but the THD% results are a little higher for the PI control.

**MP Voltage Control Algorithm**

The last voltage control algorithm implemented was the MP. As for the PI and for PR voltage control algorithms, the simulation for testing MP voltage control algorithms use a linear load and a nonlinear load. The loads have the same values as used for the other control under study. Also, at 0.25 s it is added the nonlinear load to the linear load previously used. In Fig. 9 are presented the results of this simulation with the linear and nonlinear loads using the MP voltage control algorithm for VSI.

**Fig. 9.** VSI output voltages and load currents with MP voltage control algorithm.

Analyzing the results it was possible to validate the MP voltage control algorithm for the VSI to produce three-phase sinusoidal voltages. In terms of THD% results, in Table 4, is possible to conclude the increasing values with linear load to nonlinear load. Comparing these THD% voltage results with the values obtained for the other two controls, the MP voltage control algorithm presents the higher values. Although, the THD% results are very satisfactory.

**Table 4.** MP voltage control THD% comparison using different loads.

| Load | Voltage | THD% |
|---|---|---|
| Linear | $v_{LA}$ | 1.21% |
| | $v_{LB}$ | 1.18% |
| | $v_{LC}$ | 1.18% |
| Linear + Nonlinear | $v_{LA}$ | 1.35% |
| | $v_{LB}$ | 1.31% |
| | $v_{LC}$ | 1.30% |

## 4.2    Current Controlled VSI

For the simulation of current control algorithms, the electrical schematic is presented in Fig. 10. The component values are the same as those used in the previous section. In this, the VSI is responsible for injecting energy into a three-phase 400 V/50 Hz power grid from its DC-Link (in this case using DC energy sources).

The simulation conditions are the same for all the three algorithms under study. A perturbation was caused (the reference current increases to double) to verify the response of each of the current control algorithms. Variation of current in a system is quite common as for example as the resulting from the solar radiation or wind speed change in a renewable energy application.
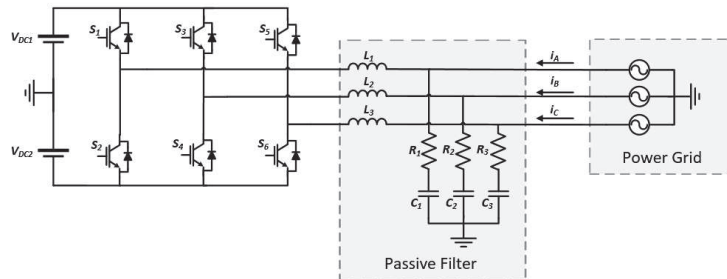


**Fig. 10.** Electrical diagram of the circuit that integrates the current-controlled VSI.

**PI Current Control Algorithm**

In Fig.11 are represented the results obtained with the application of the PI algorithm to current control. As can be seen, the PI current control algorithm causes a current spike when the references change. This spike is approximately 17 A (considering peak values) and it is evidenced in phase B because it is the phase in which the current takes the highest value at the time of the references change. These results are obtained using a $K_p$ of 100 and a $K_i$ of 15.
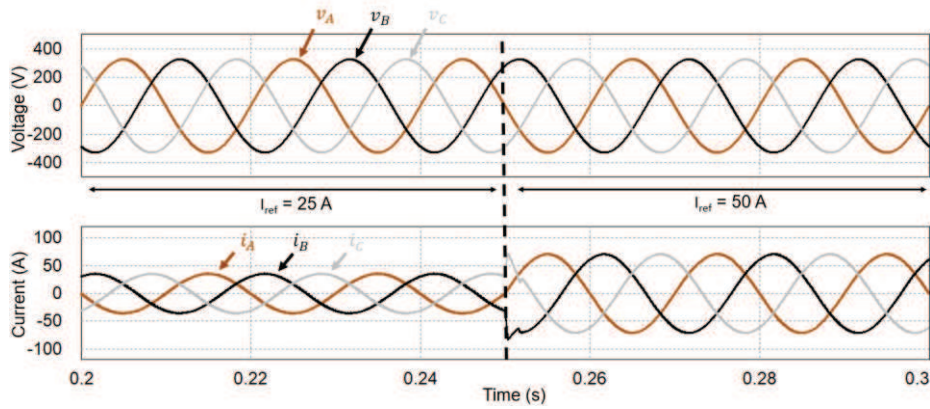
**Fig. 11.** Power grid voltages and VSI currents with PI current control algorithm.

Analyzing the results, it is possible to validate the PI current control algorithm for the VSI to inject energy into the power grid. In terms of THD% results, in Table 5, is possible to conclude the decreasing values with the increase of the current reference because the impact of switching noise is less with higher amplitude.

**Table 5.** PI current control THD% comparison using different reference amplitudes.

| Reference | Current | THD% |
|-----------|---------|------|
| 25 A | $i_A$ | 2.31% |
| | $i_B$ | 2.32% |
| | $i_C$ | 2.30% |
| 50 A | $i_A$ | 1.22% |
| | $i_B$ | 1.23% |
| | $i_C$ | 1.21% |

**PR Current Control Algorithm**

The simulation results for the PR current control algorithm are shown in Fig. 12. Like the previous algorithm, it occurs a current spike in the references change. In this case, this phenomenon has an amplitude of 9 A. These results are obtained using a $K_p$ of 120 and a $K_s$ of 800.
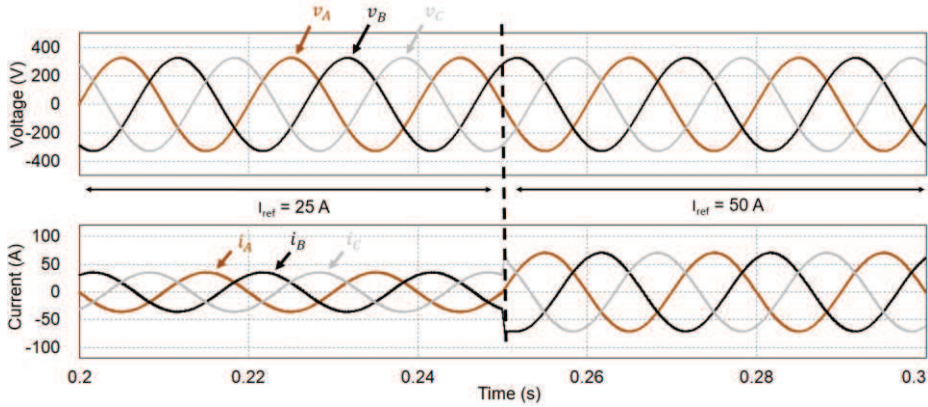
**Fig. 12.** Power grid voltages and VSI currents with PR current control algorithm.

This control produced similar results to the PI current control algorithm. The THD% results are similar, with the same behavior as in the previous control, as it can be seen in Table 6.

**Table 6.** PR current control THD% comparison using different reference amplitudes.

| Reference | Current | THD% |
|---|---|---|
| | $i_A$ | 2.29% |
| 25 A | $i_B$ | 2.32% |
| | $i_C$ | 2.27% |
| | $i_A$ | 1.18% |
| 50 A | $i_B$ | 1.20% |
| | $i_C$ | 1.17% |

**MP Current Control Algorithm**

The Fig. 13 shows the simulation results obtained by applying the MP current control algorithm. This algorithm does not cause current spikes during the references change transient, resulting in a smoother behavior.
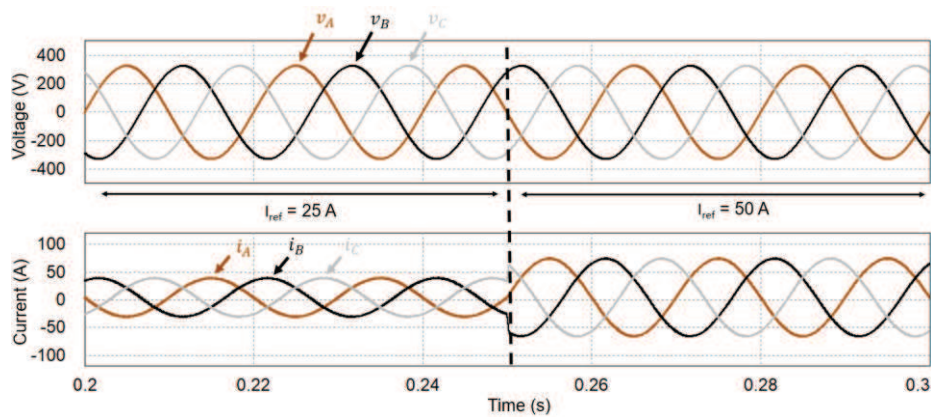
**Fig. 13.** Power grid voltages and VSI currents with MP current control algorithm.

In terms of results, the MP control algorithm has the most advantages over previous current control algorithms. It has a lower THD, being able to synthesize currents with less than 1 % THD% with a 50 A reference, as shown in Table 7.

**Table 7.** MP current control THD% comparison using different reference amplitudes.

| Reference | Current | THD% |
|-----------|---------|------|
|           | $i_A$   | 1.81 % |
| 25 A      | $i_B$   | 1.86 % |
|           | $i_C$   | 1.79 % |
|           | $i_A$   | 0.91 % |
| 50 A      | $i_B$   | 0.96 % |
|           | $i_C$   | 0.91 % |

The PI and PR voltage control algorithms present a problem. If the gains are static, variations in the reference can cause current peaks. The predictive algorithm does not have this disadvantage. However, the application of this algorithm is more complicated than the others since, in a real system, the components that constitute a converter are not ideals, making obtaining an accurate electrical model of the system a difficult process.

## 4.3    Comparative Analyses

Table 8 shows the comparison between the three control algorithms in voltage control. In terms of harmonic distortion, the algorithms are quite similar, with the PR showing slightly better results. Regarding the difficulty of implementation, the PI and PR algorithms are similar, with the MP being slightly more complex due to obtaining the system model.

**Table 8.** Comparison between the results of control algorithms in voltage control.

| Control Algorithm | THD% (Average) | Implementation Complexity |
|---|---|---|
| PI | 1.25% | Moderate |
| PR | 1.15% | Moderate |
| MP | 1.25% | Moderate/High |

Table 9 shows the comparison of the results of the application of the three algorithms in current control. The implementation difficulty is like the in the voltage control. In terms of THD% the MP control gives slightly better results. Furthermore, this algorithm does not cause current spikes, unlike PI and PR. The PI is the one with the largest current spike of 17 A.

**Table 9.** Comparison between the results of control algorithms in current control.

| Control Algorithm | THD% (Average) | Implementation Complexity | Current Transient (Overcurrent) |
|---|---|---|---|
| PI | 1.75% | Moderate | 17 A |
| PR | 1.75% | Moderate | 9 A |
| MP | 1.35% | Moderate/High | 0 A |

## 5    Conclusions

This paper compared the performance of three control algorithms for voltage source inverter (VSI). The Proportional Integral (PI), Proportional Resonant (PR) and the Model Predictive (MP) control algorithms were applied for voltage control and current control. As demonstrated in the simulations, all algorithms show good results in terms of Total Harmonic Distortion (THD%), and as expected, the THD% decreases with increasing current amplitude.

In the voltage controlled, the PR control algorithm gives slightly better results in terms of THD%. The implementation difficulty is similar for PI and PR control, the MP being slightly more difficult to implement.

In the current control, the PI and PR algorithms show very similar results, and since they have static gains, they cause an overcurrent transient in the current references change because the error is too high at this instant. The MP algorithm shows better results with respect to the transient. It also has a lower THD% in the current control. Nevertheless, it should be noted that this algorithm only works well with a good model of the electrical system, which, depending on the case, can be difficult to obtain. As future work it is planned to validate experimentally the three control algorithms to have a better perception of their behavior in real application in comparison with the simulation results.

## Acknowledgements

## References

[1] G. Zhang, Z. Li, B. Zhang, and W. A. Halang, "Power Electronics Converters: Past, Present and Future," *Renewable and Sustainable Energy Reviews*, vol. 81, pp. 2028–2044, 2018, doi: 10.1016/j.rser.2017.05.290.

[2] L. A. Barros, M. Tanta, T. J. Sousa, J. L. Afonso, and J. Pinto, "New Multifunctional Isolated Microinverter with Integrated Energy Storage System for PV Applications," *Energies*, vol. 13, no. 15, p. 4016, 2020, doi: 10.3390/en13154016.

[3] R. E. G. Duarte, L. Moreira, L. A. M. Barros, V. D. F. Monteiro, J. L. Afonso, and J. Pinto, "Power Converters for a Small Islanded Microgrid based on a Micro Wind Turbine and an Battery Energy Storage System," 2018, ISBN: 978-972-99596-4-6.

[4] D. Uma and K. Vijayarekha, "Modeling and Simulation of VSI Fed Induction Motor Drive in Matlab/Simulink," *International Journal of Electrical and Computer Engineering*, vol. 7, no. 2, p. 584, 2017, doi: 10.11591/ijece.v7i2.pp584-595.

[5] J. Pinto, V. Monteiro, H. Gonçalves, and J. L. Afonso, "Onboard Reconfigurable Battery Charger for Electric Vehicles with Traction-to-Auxiliary Mode," *IEEE Transactions on vehicular technology*, vol. 63, no. 3, pp. 1104–1116, 2013, doi: 10.1109/TVT.2013.2283531.

[6] S. Azmi, K. Ahmed, S. Finney, and B. Williams, "Comparative Analysis Between Voltage and Current Source Inverters in Grid-Connected Application," 2011, doi: 10.1049/cp.2011.0138.

[7] A. Sarkar, "Modeling and Control of a Three Phase Voltage Source Inverter with an LCL Filter," Arizona State University, 2015.

[8] R. Mandrioli, M. Hammami, A. Viatkin, R. Barbone, D. Pontara, and M. Ricco, "Phase and Neutral Current Ripple Analysis in Three-Phase Four-Wire Split-Capacitor Grid Converter for EV Chargers," *Electronics*, vol. 10, no. 9, p. 1016, 2021, doi: 10.3390/electronics10091016.

[9] T. D. Castillo and J. R. Castro, "Renewable Energy Source PV connected to the grid through Shunt Active Power Filter based in PQ Theory," *2018 IEEE Third Ecuador Technical Chapters Meeting (ETCM)*, pp. 1–5, 2018, doi: 10.1109/ETCM.2018.8580274.

[10] A. Y. Mohammed, F. I. Mohammed, and M. Y. Ibrahim, "Grid connected Photovoltaic system," in *2017 International Conference on Communication, Control, Computing and Electronics Engineering (ICCCCEE)*, 2017, pp. 1–5, doi: 10.1109/ICCCCEE.2017.7867659.

[11] K. Milev, V. Yaramasu, A. Dekka, and S. Kouro, "Predictive Control of Multichannel Boost Converter and VSI-Based Six-Phase PMSG Wind Energy Systems with Fixed Switching Frequency," in *2020 11th Power Electronics, Drive Systems, and Technologies Conference (PEDSTC)*, 2020, pp. 1–6, doi: 10.1109/PEDSTC49159.2020.9088419.

[12] P. Mishra, S. Munk-Neilsen, and R. Maheshwari, "Testing of SiC Voltage Source Inverter Fed Induction Motor Drive and its Control with Output Sinusoidal LC Filter," in *2020

*IEEE International Conference on Power Electronics, Drives and Energy Systems (PEDES)*, 2020, pp. 1–5, doi: 10.1109/PEDES49360.2020.9379605.

[13] M. R. Haque and S. Khan, "The Modified Proportional Integral Controller for the BLDC Motor and Electric Vehicle," in *2021 IEEE International IOT, Electronics and Mechatronics Conference (IEMTRONICS)*, 2021, pp. 1–5, doi: 10.1109/IEMTRONICS52119.2021.9422548.

[14] A. Ortiz, M. Aredes, L. G. Rolim, E. Bueno, and P. Rodriguez, "A New Current Control for the STATCOM based on Secondary Order Generalized Integrators," *2008 IEEE Power Electronics Specialists Conference*, pp. 1378–1383, 2008.

[15] P. Santiprapan, K. Areerak, and K. Areerak, "Proportional plus Resonant Control for Active Power Filter in Unbalanced System," in *2017 International Electrical Engineering Congress (iEECON)*, 2017, pp. 1–4, doi: 10.1109/IEECON.2017.8075733.

[16] O. Abdel-Rahim and H. Furiato, "Switched Inductor Quadratic Boosting Ratio Inverter with Proportional Resonant Controller for Grid-Tie PV Applications," *IECON 2014-40th Annual Conference of the IEEE Industrial Electronics Society*, pp. 5606–5611, 2014, doi: 10.1109/IECON.2014.7049358.

[17] A. Pirooz and R. Noroozian, "Predictive Voltage Control of Three-Phase Voltage Source Inverters to Supply Nonlinear and Unbalanced Loads," in *The 6th Power Electronics, Drive Systems & Technologies Conference (PEDSTC2015)*, 2015, pp. 389–394.

[18] H. Shi, J. Zong, and L. Ren, "Modified Model Predictive Control of Voltage Source Inverter," in *2019 IEEE 4th Advanced Information Technology, Electronic and Automation Control Conference (IAEAC)*, 2019, vol. 1, pp. 754–759, doi: 10.1109/IAEAC47372.2019.8997737.

[19] J. L. A. Vitor Monteiro and A. A. N. Meléndez, "Novel Single-Phase Five-Level VIENNA-Type Rectifier with Model Predictive Current Control," *IECON 2017-43rd Annual Conference of the IEEE Industrial Electronics Society*, pp. 6413–6418, 2017.

[20] B. Boukezata, A. Chaoui, J.-P. Gaubert, and M. Hachemi, "Implementation of Predictive Current Control for Shunt Active Power Filter," *2017 6th International Conference on Systems and Control (ICSC)*, pp. 133–138, 2017.